Ultrathin GaN quantum wells in AlN nanowires for UV-C emission

Rémy Vermeersch, Gwénolé Jacopin, Florian Castioni, Jean-Luc Rouvière, Alberto Garcia-Cristobal, Ana Cros, Julien Pernot, Bruno Daudin

Ultrathin GaN quantum wells in AlN nanowires for UV-C emission

Rémy Vermeersch[1,2], Gwénolé Jacopin[1], F. Castioni[3], J. L. Rouvière[4], A. García-Cristóbal[5], A. Cros[5], Julien Pernot[1], Bruno Daudin[2]

[1] Univ. Grenoble Alpes, Grenoble INP, CNRS, Institut Néel , 38000 Grenoble, France.

[2] Univ. Grenoble Alpes, Grenoble INP, CEA, IRIG-PHELIQS, NPSC, 17 rue des martyrs, 38000 Grenoble, France.

[3] Univ. Grenoble Alpes, CEA, LETI, 17 rue des martyrs, 38000 Grenoble, France

[4] Univ. Grenoble Alpes, Grenoble INP, CEA, IRIG-MEM, LEMMA, 17 rue des martyrs, 38000 Grenoble, France.

[5] Materials Science Institute (ICMUV), University of Valencia, ES-46071 Valencia, Spain

Corresponding author: bruno.daudin@cea.fr

Abstract

Molecular beam epitaxy growth and optical properties of GaN quantum disks in AlN nanowires were investigated, with the purpose of controlling the emission wavelength of AlN nanowire-based light emitting diodes. Besides GaN quantum disks with a thickness ranging from 1 to 4 monolayers, a special attention was paid to incomplete GaN disks exhibiting lateral confinement. Their emission consists of sharp lines which extend down to 215 nm, in the vicinity of AlN band edge. The room temperature cathodoluminescence intensity of an ensemble of GaN quantum disks embedded in AlN nanowires is about 20 % of the low temperature value, emphasizing the potential of ultrathin/incomplete GaN quantum disks for deep UV emission.

The current interest in UV-C emitters is partly motivated by applications such as surface and skin disinfection as well as air and water purification.[1] These sanitization applications require UV emission in the 230 - 280 nm range, in order to optimally cover the DNA absorption band. The direct wide band gap of GaN (3.5 eV) and AlN (6.2 eV) makes ternary AlGaN alloys particularly attractive to cover these applications, despite the relatively poor efficiency of current UV-C light emitting diodes (LEDs).[1] To overcome some of the limitations of layer UV-C LEDs, namely the poor p-type doping and the presence in layers of extended defects caused by the lack of lattice-matched substrates, III-N nanowire (NW) heterostructures appear as a promising option. The eased elastic strain relaxation in NWs provided their diameter is small enough [2] combined to the expected increased dopant solubility paved the way to the recent realization of NW-based UV-C LEDs, including AlN/AlGaN/AlN NW heterostructures. [3–5]. However, the composition control of thin AlGaN NW sections required for tuning the active region emission wavelength is problematic: the random formation of spontaneous GaN/AlN superlattices, which is related to the nucleation mechanism of successive layers in NWs, makes difficult the realization of AlGaN quantum wells (QWs) in NWs, which should be controlled in both thickness and composition. [6–8]

As recently demonstrated, the growth of short period GaN/AlN superlattices (SPSLs) allows one to overcome this obstacle. [9,10] Besides allowing one to accommodate the lattice mismatch between AlN barriers and the active region, the tuning of the *m*AlN/*n*GaN section, were *m* and *n* correspond to the number of monolayers (MLs) of AlN and GaN deposited, respectively, allows one to adjust the composition of the equivalent AlGaN alloy and the expected wavelength emission down to 225 nm [11] and even 219 nm if using sub-ML (0.8 ML thick) GaN QWs, which exhibit a high luminescence efficiency. [12]

This paradigm seems promising to precisely control the emission energy in NW geometry and overcome the problematic AlGaN growth issue described here above. However, a controlled growth at the ML scale of an array of spontaneously nucleated NW is challenging as every single wire receives additional atomic flux coming from its sidewalls, which is modulated by the shadow effect of surrounding NWs. In the special case of GaN/AlN NW heterostructures, the short diffusion length of Al along the side walls with respect to its Ga counterpart leads to the formation of an AlN shell around the GaN/AlN superlattice core. [13,14] As a result, the GaN QWs -sometimes denominated quantum disks (QDKs) in this

specific case- are then experiencing a strain state with an axial component, differentiating them from the QWs embedded in AlN layers. [13] The goal of the present article was to focus on the case of ultra-thin –from submonolayer to some MLs – GaN QDKs in such NW AlN/GaN heterostructures. More precisely, our purpose was to investigate the way their specific strain state could affect their optical properties and evaluate their potential for UV-C emission.

The GaN/AlN NWs heterostructures sample were grown by plasma-assisted MBE on highly conductive n-type (111)-Si substrate, which leads to the spontaneous nucleation of (000-1) oriented (i.e. N-polar) NWs. [15] These heterostructures consisted of a 500 nm long GaN stem, followed by the growth of a 200 nm long AlN section. Next, the GaN/AlN QWs section was grown by alternated exposure to metal and nitrogen fluxes, allowing eased metal diffusion on the top surface prior to nitridation of the metallic layer. This technique is used in order to obtain a better control of the adatom density on the growth front and allows for a better control of the growth at the ML scale. [12] Two samples were investigated. Sample A consisted of a 60 periods AlN/GaN superlattice. The GaN QW sequence was (14s Ga / 14s N) and the barrier sequence (30s Al / 30s N/ 25s Al / 30s N). The N (respectively Al/Ga) flux was 0.16 ML/s (respectively 0.1 ML/s), deduced from RHEED oscillation calibration. The same fluxes were used for growing sample B, which consisted of a 40 periods AlN/GaN superlattice. The GaN QW sequence was 2 x (14s Ga / 14s N) and the barrier sequence 30s Al / (30s N / 25s Al / 30s N). Growth temperature was 800 °C (respectively 750°C) for sample A (respectively B). The samples were analyzed using scanning transmission electron microscopy (STEM) in a probe corrected TFS Titan Themis microscope operating at 200 kV. The observations were realized using high-angle annular dark field (HAADF) detector, the obtained image contrast being directly dependent on the chemical composition. In order to increase the signal-to-noise ratio and reduce the sample instabilities, atomic-scale STEM-HAADF images were obtained following a multi-frame approach with a fast acquisition time followed by a stack registration to correct spatial drift.[16] Optical properties were assessed by the mean of cathodoluminescence (CL) which was done in a FEI Inspect F50 scanning electron microscope (SEM). The signal was detected through a Horiba Jobin Yvon iHR 550 spectrometer equipped with 1800 grooves.mm^{-1} gratings (0.013 nm/pixel) and a Peltier-cooled Andor Technology Newton DU940 CCD. The beam size was of around 20 nm in diameter and an acceleration voltage between 10 and 20 kV was applied corresponding to an interaction region depth larger than 750 nm.

Figure 1a shows a high angle annular dark field (HAADF) scanning transmission electron microscopy (STEM) image of sample A. The GaN QWs (light contrast) are 1 ML thick while the AlN barrier is about 7 MLs thick. Both show slight random thickness fluctuations of one ML. The room temperature cathodoluminescence (CL) performed on an ensemble of NWs, shown in figure 1b, is dominated by a peak at 240 nm, assigned to 1 ML thick GaN QWs. The long wavelength shoulder is consistent with QWs thickness fluctuations. In particular, the contribution at about 265 nm corresponds to 2 GaN MLs, as will be discussed later. CL measurement is averaged over ~10.000 NWs, which emphasizes the good control and homogeneity of GaN QW thickness from wire to wire, thanks to the use of alternated flux during the growth of the active area.

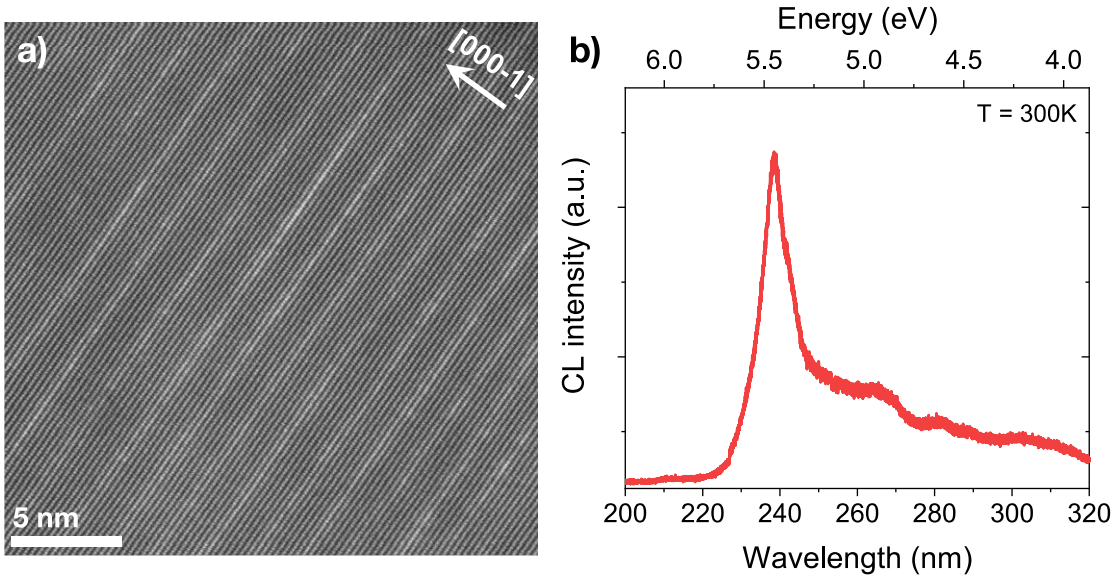

Figure 1: a) STEM-HAADF image of the monolayer thin GaN quantum well in AlN barriers of sample A. b) Room-temperature CL spectrum of sample A.

Taking advantage of the decreasing temperature gradient from wafer center to the edge in sample B, which is correlated to a continuous increase of the adsorbed Ga amount from the centre to the edge, GaN QWs of different thickness were grown on the same wafer. Nevertheless, as a consequence of the negligible Al desorption rate in the 700-800°C growth temperature range, no significant variations in the AlN barrier thickness are expected. CL experiments performed on different locations between 15 and 24 mm along the wafer diameter are plotted in figure 2. Interestingly, four discrete peaks are visible, progressively red shifting as the growth temperature decreases. These peaks at 239, 267, 289 and 304 nm,

are assigned to the emission of QW of thickness 1, 2, 3 and 4 MLs. On the same figure are plotted the room-temperature CL spectra. One can still clearly identify these peaks with almost no shifts in the emission wavelength, indicative of a reduced CL temperature quenching, which is assigned to strong exciton localization, possibly mediated by nanoscale atomic roughness of the GaN QWs.[17,18]

Remarkably the CL spectrum recorded at 15 mm from the wafer center on a bunch of about 15 NWs exhibits sharp lines superimposed on a band corresponding to the emission of one ML GaN QWs, without additional CL signature of thicker QWs. This specific luminescence behaviour will be discussed later.

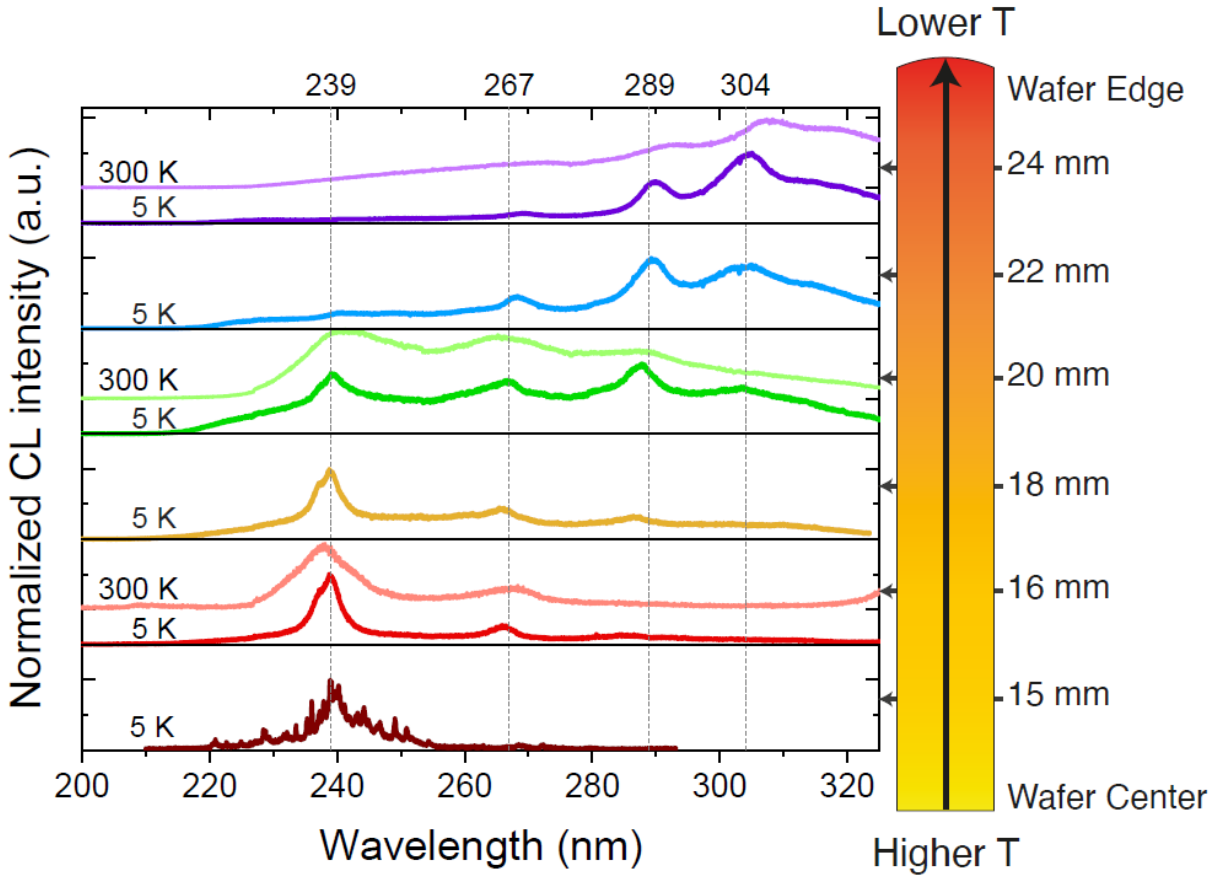

Figure 2: Normalized CL spectra of sample B for various positions along the wafer. CL spectra are averaged over around 10.000 NWs except for the dark brown spectrum (15 mm position) which corresponds to around 15 NWs. Thick lines are measured at 5 K. When present, thin lines are measured at 300 K. The dotted vertical lines correspond to the different peaks assigned to 1-4 MLs of GaN. Right cartoon represents a wafer slice with the positions at which CL signal was acquired.

Figure 3 shows the optical properties at the 20 mm position. Figure 3.a presents CL spectrum as a function of temperature, highlighting the coexistence of the four QW thicknesses. Peaks at 360 and 380 nm are attributed to GaN-related recombinations. The integrated CL intensity around the three lower wavelength peaks, marked with colored stars, is further plotted as function of the temperature in Figure 3.b. The three peaks present a similar behavior with room temperature intensity around 20 % of the one at 5 K, confirming the low quenching of the luminescence and efficient radiative carrier recombination. Moreover, the loss in luminescence intensity is found to be independent from the GaN well thickness in the 1 to 3 MLs range.

Low-temperature CL mapping were acquired on an array of NWs which is shown in Figure 3.c. Figure 3.d shows the mapping at the GaN band-edge emission. NWs can clearly be distinguished without large variations in CL intensity. Figure 3.e. shows an hyper spectral map where the RGB color code corresponds to the three peaks marked in Figure 3.a. From this spectral map, it is concluded that most individual NWs mainly exhibit a single emission peak corresponding to a specific GaN QW thickness and not to QW thickness variations within the same NW. These fluctuations from NW to NW are assigned to local fluctuations in the amount of adsorbed Ga. Indeed, it is well established that the effective Ga flux on top of the NWs results from a balance between Ga flux directly impinging on top, Ga flux resulting from side wall diffusion to the top and temperature-dependent desorbing Ga flux from top.[19,20] In the present case of spontaneously nucleated NWs on Si, random diameter fluctuations and variable shadow effects associated with random NW spacing are affecting the local amount of Ga available on NW top and consequently the GaN QW thickness from NW to NW.

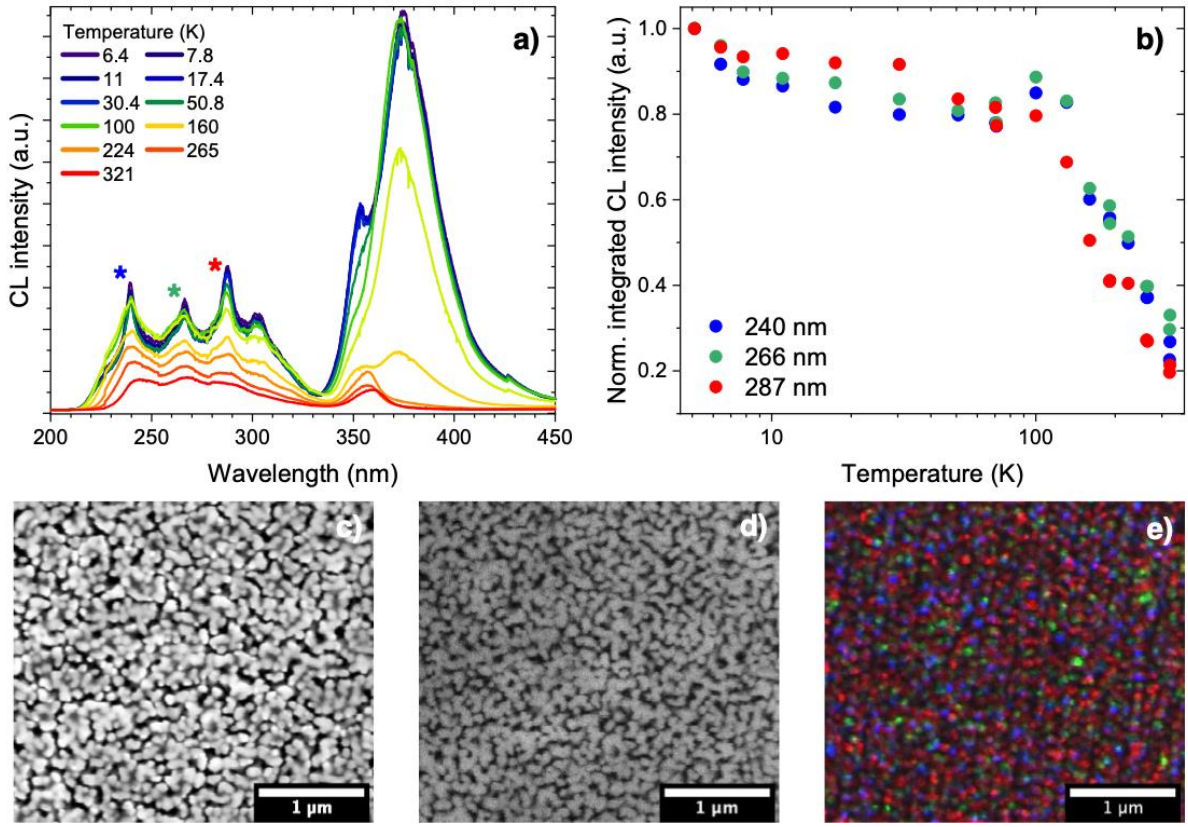

Figure 3: a) Temperature dependent CL spectra of Sample B at the position denoted "20 mm" in Figure 2. Stars denote the peaks used in (b) and (e). b) Integrated CL spectra as function of the temperature. The integration bounds are ± 5 nm centered at the peak position indicated in the caption. c) Secondary electron image of the scanned area for (d-e). d) CL map at 370 nm. e) Hyper spectral CL map of the area. Blue: 240 nm, green: 266 nm, red: 287 nm. Spectral window for maps in (d) and (e) is of ± 3 nm.

In order to shed light on the features observed at the 15 mm location, additional CL experiments were performed on two joined NWs obtained by dispersion of NWs from this area on a TEM grid. CL spectra displayed in Figure 4.a-b. show a wide variety of thin emission lines extending down to 215 nm. This collection of sharp line indicates the presence of nanometric recombination centers able to strongly localize the exciton in a quantum dot manner. The inset of Figure 4.a, which represents a CL mapping of the two NWs at 228, 239 and 257 nm, allows one to identify areas at the NW scale which emit at these specific wavelengths. Further STEM- HAADF analysis shown in Figure 4.c confirmed the presence of incomplete QWs, extending well below the whole NW diameter. The formation of such QWs is probably due to enhanced Ga desorption in this region, associated with higher growth

temperature. Accordingly, the emission lines observed below 240 nm (which corresponds to 1 ML) are assigned to the recombination of confined carriers in these incomplete QWs, with a lateral size smaller or comparable to the 2.8 nm GaN Bohr exciton radius. Emission lines above 240 nm are attributed to larger 3D GaN clusters which have also been observed [21]. They are however out of the scope of this study.

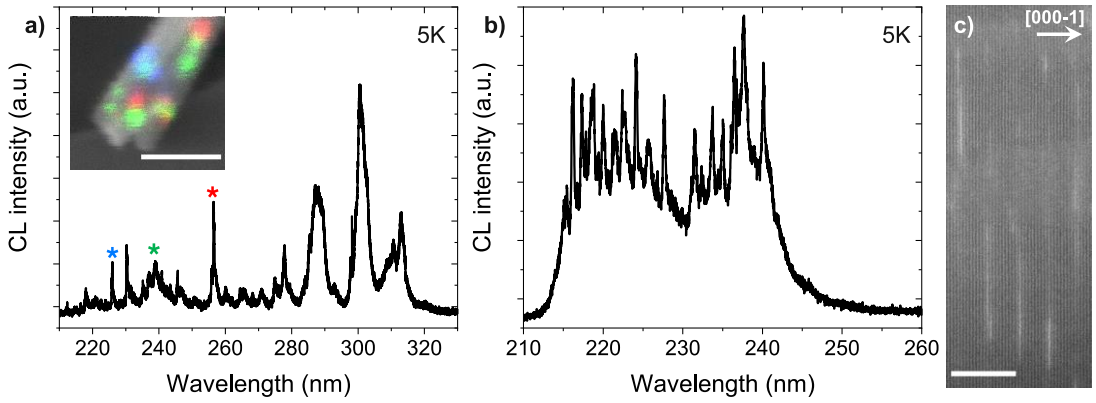

Figure 4: (a) 5K CL spectrum of two single NWs shown in the inset. The color code refers to different spots emitting at different wavelengths. The peak at 240 nm is assigned to 1 ML thick GaN QWs. The scale bar in the inset is 200 nm. (b) 5K CL spectrum in another spot, emphasizing the presence of sharp lines below 240 nm, which are assigned to the presence of incomplete QWs. (c) STEM-HAADF image of the incomplete GaN QWs. The scale bar is 5 nm.

A mechanism accounting for the growth of incomplete GaN QWs is schematized in Figure 5. For a growth temperature high enough, the weak sticking coefficient of Ga with respect to Al as well as the stronger Al-N bond with respect to its Ga-N counterpart result in pure AlN growth and progressive accumulation of Ga on the surface as a consequence of the low GaN nucleation probability, when the growth front is *continuously* exposed to a Ga flux. Eventually, for a Ga adatom density high enough, GaN nucleation is *randomly* triggered, followed by the consumption of the Ga reservoir available on the NW top surface. Following layer completion and further AlN growth, this process is spontaneously repeated, leading to the formation of a stack of incomplete GaN QWs with random lateral size. This kinetically driven mechanism is likely responsible for the spontaneous formation of random GaN/AlN superlattices in NWs in the case of a Ga amount sufficient for growth of complete GaN layers alternating with AlN.[22]

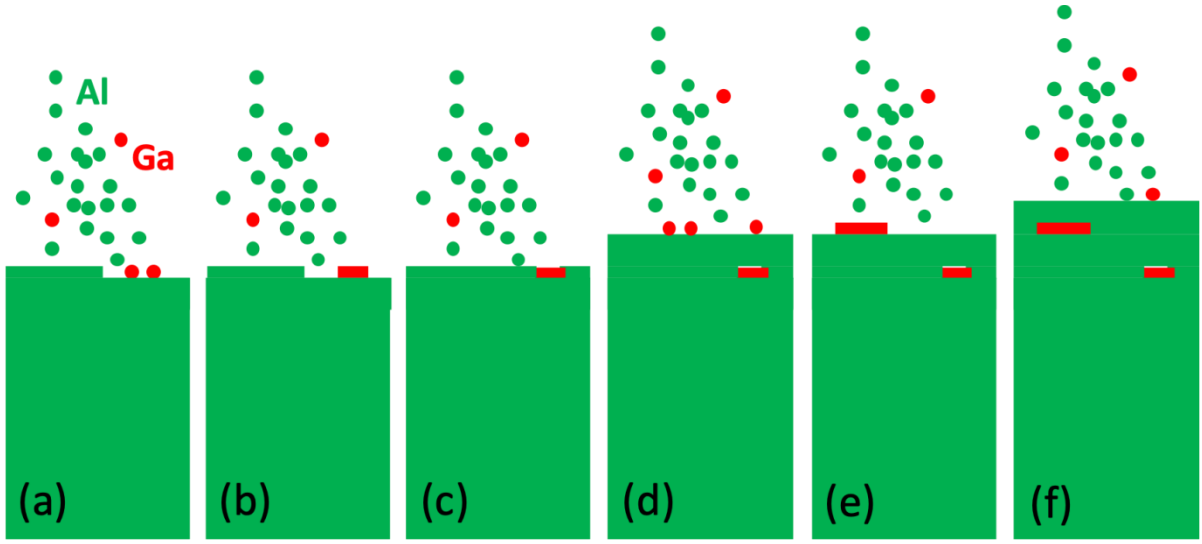

Figure 5: (a) Growing AlN NW under a Ga flux exposure leading to progressive Ga accumulation on top until (b) the onset of GaN nucleation and Ga reservoir consumption, (c) followed by further AlN growth and (d), (e), (f) cycle repetition.

By contrast, in the case of the present study, the growing AlN NWs are *periodically* exposed to a Ga flux, as mentioned above. Depending on the growth temperature and, consequently, on the Ga sticking coefficient, this results in the formation of GaN QWs with a thickness in the 1-4 MLs range, as shown in figure 2. However, if the amount of Ga accumulated on the surface turns to be lower than 1 ML, it may lead to the random formation of incomplete QWs, as shown in figure 4.c, the nucleation of which is *periodically* triggered by the abrupt change in Ga adatom density on the growth front resulting from *periodical* exposure to Ga flux. The collection of sharp emission lines observed at wavelength lower than 239 nm in figure 4.b, i.e. lower than the emission peak corresponding to 1 ML thick GaN QWs, is assigned to the presence of such incomplete, strongly confining QWs of randomly distributed lateral size, in agreement with the schematic in Figure 5.

One factor a priori influencing the emission energy is the strain state of the system. In this respect, it is worth noting that the strain state of the GaN QDKs embedded in the nanowires might be different from that found in equivalent 2D GaN/AlN superlattices (SLs). In the latter case, an ideal pseudomorphic growth implies a constant biaxial strain. The actual in-plane parameter value adopted by the SL depends on the substrate nature and the value of both GaN and AlN layer thickness. It ranges from a value fixed by the thick substrate on which the system is grown to an average parameter between the values of GaN and AlN if

one can consider the SL as free-standing, i.e. decoupled from the substrate. In contrast, in the case of GaN QDKs in a NW, the finite lateral extension of the system (and, in our case, the additional presence of an AlN shell) will give rise to a more complicated strain distribution. In order to unravel the differences with respect to the case of infinite 2D layers, we have performed finite element method (FEM) simulations of the strain field in a realistic model of the investigated system. Following the results obtained by TEM, we have considered the geometry shown in Figure 6.a, consisting of a series of GaN disks embedded in a nanowire. The shell observed in the experiments is accounted for by taking different radii of the disks and the wire. As the 200 nm long AlN section on top of the 500 nm GaN stem is expected to be fully relaxed in our samples, in the simulations we assume that the bottom end of the NW adopts the AlN in-plane lattice parameter. In Figure 6.b we show the strain components along the wire axis for a NW containing 40 disks (as in sample B). For comparison we also display in Figure 6.b the results for an equivalent 2D GaN/AlN SL lattice matched to AlN. The results of Figure 6.b clearly show that the possibility of lateral strain relaxation at the NW surface, combined with the constraining AlN shell, leads to a completely different picture of the strain as compared to the 2D SL. These differences are more pronounced for the system of 4 ML GaN QWs, and are progressively reduced as we decrease the thickness to 1 ML. From the results in Fig. 6 we have calculated, by means of an appropriate ***k.p*** (effective mass) Hamiltonian, the strain-modified conduction and valence band edge profiles of the structure along the axis (not shown). Our results indicate that, despite the numerical differences in the strain, the resulting energy profile is almost the same in both systems, GaN QDKs and 2D SL. Accordingly, the local GaN gap is essentially the same for all disks within a NW and differs from that of the 2D SL by no more than 20 meV. Therefore, the main role to account for the optical transition energies is expected to be played by the confinement effects within the GaN disks.

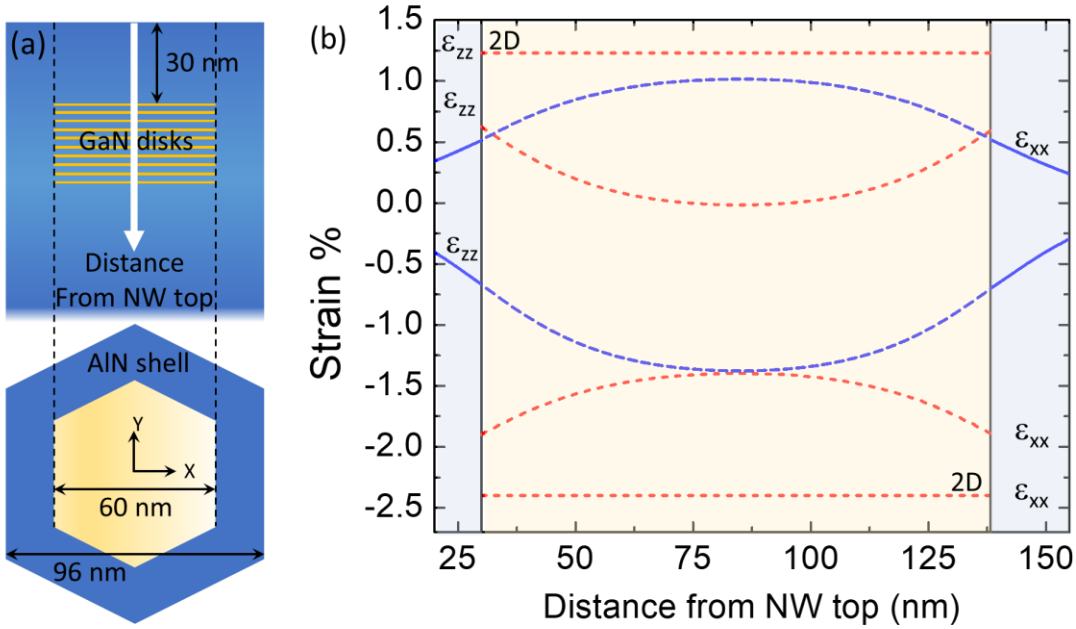

Figure 6: (a) Geometry of the simulated system of GaN QDKs embedded in an AlN nanowire. A sequence of 10 disks is displayed here but the calculations are performed for a sequence of 40 disks, as in sample B. All dimensions are obtained from TEM pictures. The thickness of the AlN barrier between the disks is 7 ML. The thickness of the GaN disks is here 4ML, but simulations have been performed for thicknesses of 1 to 4 ML. (b) Components of the local strain (ε_{xx} and ε_{zz}, in %) along the NW axis, for the system of 4 ML high disks. GaN strain is displayed in red, AlN strain in blue. The horizontal lines correspond to the GaN strain in a 2D GaN/AlN SL with the same vertical dimensions. In this 2D SL, AlN is relaxed.

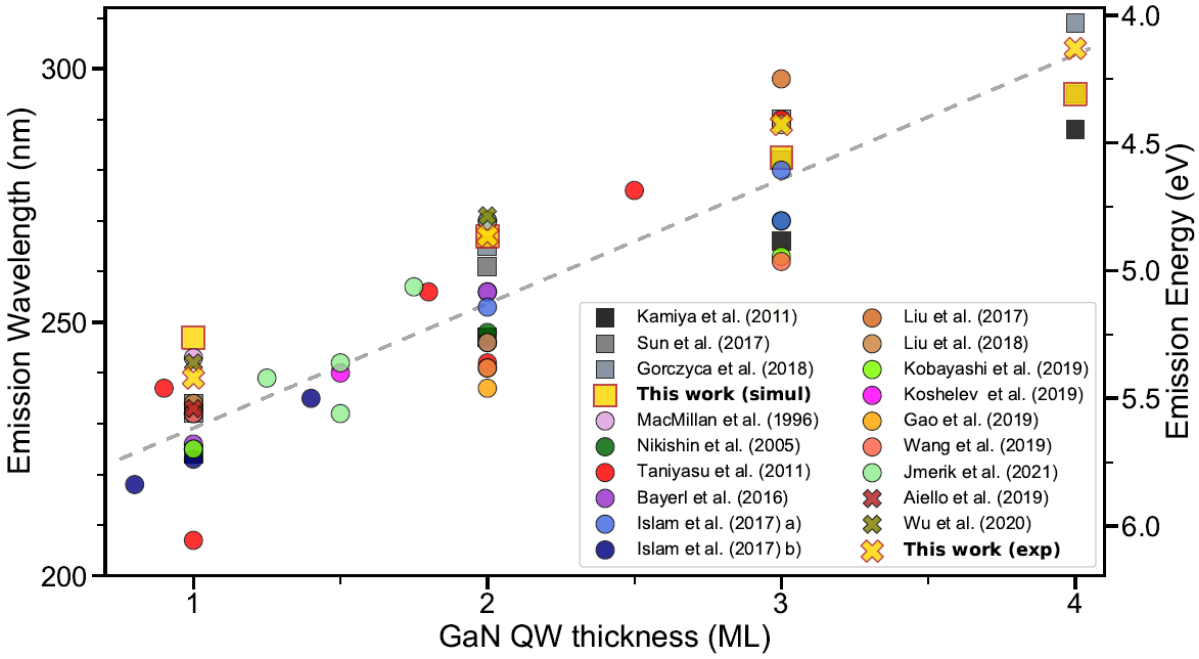

Figure 7: Literature review of emission wavelength as function of the GaN QW thickness. Circles indicate experimental results from 2D layers, crosses from nanowires and squares from theoretical simulations. Grey dashed line is a guide for the eye.

The results of the present study for the emission energies are plotted in Figure 7 along with a review of data reported in the literature, which refer to GaN/AlN superlattices in layers [11,12,23–33] and NWs [34,35]. In order to have an accurate theoretical value of the optical transition energies one should calculate the confined states in the system of disks, under the strain-modified position-dependent band profiles, and probably also include excitonic effects. This is outside the scope of this work. We have instead estimated them by calculating the confinement energies of the lowest electron state (those of the hole are virtually zero given its extremely heavy mass) in a 2D SL (with the strain state extracted from the central disk in the previous calculations, see Fig. 6) and adding them to the corresponding strain-modified GaN band gap. Note that the electric field is neglected here, in regards of the small dimension of the wells. The so obtained results are also displayed in Fig. 7, together with those from other theoretical calculations [10,36,37]. First, it is noticeable that the estimated transition energies are in overall agreement with our experimental results. However, it also appears that either for theoretical results or experimental ones, discrepancies between reported values in literature are significant. One first reason for these discrepancies is the variability of AlN barrier thickness. Depending on it, short period GaN/AlN superlattices (SPSLs) can be viewed either

as digital alloys or as a collection of GaN wells into AlN barriers. As theoretically established by Sun et al in the case of layers, AlN barriers above a threshold thickness of 7-9 MLs behave similarly to infinite ones leading to a saturation of GaN QW emission energy. [37] Reports from the literature do not always precise the AlN barrier thickness so that data points plotted in Figure 7 refer either to single quantum well (i.e. infinitely thick AlN barriers) or to AlN barriers as thin as 4 ML in the extreme case reported by Nikishin et al. [25]. Also, the determination of GaN QW thickness may be problematic. As pointed out by Jmerik et al in particular, the presence of steps on the surface may lead to local thickening of GaN QW. [23] Accordingly, GaN QW thickness determination by X-Rays diffraction, which provides an average value at large scale, leads to non-integer values of the average GaN QW thickness, as shown in Figure 7, while emission wavelength should be rather governed in this case by the carrier localization in the thicker GaN QW regions.

Finally, it appears that the data of the present study are in good agreement with the results reported in literature. Nevertheless, as shown in Figure 7, they lay in the long wavelength region of the data cloud. Interestingly, this is also the case for the data of Aiello et al [30] and Wu et al [31], also for NWs. From the above theoretical analysis, it is concluded that the specific strain state of GaN QWs in NWs cannot account alone for the trend to red shift of our data with respect to the average emission wavelength of reported data. Indeed, in spite of significant differences between the strain state of 2D GaN/AlN SLs and the strain state of GaN QDKs in NWs, the effect on the transition energies is negligible. Increasing the AlN barrier thickness from 7 to 14 MLs, while changing the strain profile did not appreciably affect the value of the GaN QDK transition energies (not shown), which discards the effect of reduced AlN barrier thickness on the red shift trend of the transition energies observed in the present study. The residual strain state in the substrate could be a source of data dispersion in the case of layers, compared to the case of the strain-relaxed AlN section used in this work. Finally, it is also possible that the recombination energy in GaN QWs or QDKs be affected by the presence of localized states at the QW/barrier interface, which should be drastically dependent on experimental growth conditions. .

In summary, we demonstrated that the specific strain state of GaN QDKs embedded in AlN NWs with respect to their 2D GaN/AlN SLs counterpart has a limited effect on transition energies. The possible tuning of the GaN QW wavelength emission by controlling the formation of incomplete GaN QWs exhibiting a marked lateral carrier confinement was put in evidence, opening the path to the realization of UV-C emitting devices fully covering the 220-

320 nm range.

Acknowledgments: The authors thank Y. Genuist, Y. Curé, and F. Jourdan for technical support during MBE growth and F. Donatini for the support with the cathodoluminescence experimental setup. We acknowledge support from GANEXT (ANR-11-LABX-0014). GANEXT belongs to the public funded 'Investissements d'Avenir' program managed by the French ANR agency. A.C. acknowledges Generalitat Valenciana for financial support through project CIPROM2021-75. The work of A. G.-C. was performed in the framework of the project I+D+I PID2020-112507GB-I0, funded by MCIN/AEI/10.13039/501100011033 and by "ERDF A way of making Europe", and under Grant PROMETEO/2021/082 (ENIGMA), funded by Generalitat Valenciana.

References

[1] Kneissl M, Seong T-Y, Han J and Amano H 2019 The emergence and prospects of deep-ultraviolet light-emitting diode technologies *Nat. Photonics* **13** 233–44

[2] Glas F 2006 Critical dimensions for the plastic relaxation of strained axial heterostructures in free-standing nanowires *Phys. Rev. B - Condens. Matter Mater. Phys.* **74** 2–5

[3] Velpula R T, Jain B, Philip M R, Nguyen H D, Wang R and Nguyen H P T 2020 Epitaxial Growth and Characterization of AlInN-Based Core-Shell Nanowire Light Emitting Diodes Operating in the Ultraviolet Spectrum *Sci. Rep.* **10** 1–10

[4] Zhao S, Djavid M and Mi Z 2015 Surface Emitting, High Efficiency Near-Vacuum Ultraviolet Light Source with Aluminum Nitride Nanowires Monolithically Grown on Silicon *Nano Lett.* **15** 7006–9

[5] Zhao S, Connie A T, Dastjerdi M H T, Kong X H, Wang Q, Djavid M, Sadaf S, Liu X D, Shih I, Guo H and Mi Z 2015 Aluminum nitride nanowire light emitting diodes: Breaking the fundamental bottleneck of deep ultraviolet light sources *Sci. Rep.* **5** 8332

[6] Zhao S, Woo S Y, Bugnet M, Liu X, Kang J, Botton G A and Mi Z 2015 Three-Dimensional Quantum Confinement of Charge Carriers in Self-Organized AlGaN Nanowires: A Viable Route to Electrically Injected Deep Ultraviolet Lasers *Nano Lett.* **15** 7801–7

[7] Daudin B, Siladie A M, Gruart M, Den Hertog M, Bougerol C, Haas B, Rouvière J L, Robin E, Recio-Carretero M J, Garro N and Cros A 2021 The role of surface diffusion

in the growth mechanism of III-nitride nanowires and nanotubes *Nanotechnology* **32**

[8] Nemoz M, Semond F, Rennesson S, Leroux M, Bouchoule S, Patriarche G and Zuniga-Perez J 2021 Interdiffusion of Al and Ga in AlN/AlGaN superlattices grown by ammonia-assisted molecular beam epitaxy *Superlattices Microstruct.* **150** 106801

[9] Nikishin S 2018 III-Nitride Short Period Superlattices for Deep UV Light Emitters *Appl. Sci.* **8** 2362

[10] Gorczyca I, Suski T, Christensen N E and Svane A 2018 Theoretical study of nitride short period superlattices *J. Phys. Condens. Matter* **30**

[11] Bayerl D, Islam S, Jones C M, Protasenko V, Jena D and Kioupakis E 2016 Deep ultraviolet emission from ultra-thin GaN/AlN heterostructures *Appl. Phys. Lett.* **109** 241102

[12] Islam S M, Protasenko V, Lee K, Rouvimov S, Verma J, Xing H and Jena D 2017 Deep-UV emission at 219 nm from ultrathin MBE GaN/AlN quantum heterostructures *Appl. Phys. Lett.* **111** 3–7

[13] Hestroffer K, Mata R, Camacho D, Leclere C, Tourbot G, Niquet Y M, Cros A, Bougerol C, Renevier H and Daudin B 2010 The structural properties of GaN/AlN core-shell nanocolumn heterostructures *Nanotechnology* **21**

[14] Deng J, Yu J, Hao Z, Kang J, Lu B, Wang L, Sun C, Han Y, Xiong B, Wang J, Li H and Luo Y 2022 Disk-Shaped GaN Quantum Dots Embedded in AlN Nanowires for Room-Temperature Single-Photon Emitters Applicable to Quantum Information Technology *ACS Appl. Nano Mater.* **5** 4000–8

[15] Hestroffer K, Leclere C, Bougerol C, Renevier H and Daudin B 2011 Polarity of GaN nanowires grown by plasma-assisted molecular beam epitaxy on Si(111) *Phys. Rev. B* **84** 245302

[16] Jones L, Varambhia A, Beanland R, Kepaptsoglou D, Griffiths I, Ishizuka A, Azough F, Freer R, Ishizuka K, Cherns D, Ramasse Q M, Lozano-Perez S and Nellist P D 2018 Managing dose-, damage- and data-rates in multi-frame spectrum-imaging *Microscopy* **67** i98–113

[17] Rigutti L, Mancini L, Lefebvre W, Houard J, Hernàndez-Maldonado D, Di Russo E, Giraud E, Butté R, Carlin J-F, Grandjean N, Blavette D and Vurpillot F 2016 Statistical nanoscale study of localised radiative transitions in GaN/AlGaN quantum wells and AlGaN epitaxial layers *Semicond. Sci. Technol.* **31** 095009

[18] Gallart M, Morel A, Taliercio T, Lefebvre P, Gil B, Allègre J, Mathieu H, Grandjean N, Leroux M and Massies J 2000 Scale Effects on Exciton Localization and

Nonradiative Processes in GaN/AlGaN Quantum Wells *Phys. status solidi* **180** 127–32

[19] Debnath R K, Meijers R, Richter T, Stoica T, Calarco R and Lüth H 2007 Mechanism of molecular beam epitaxy growth of GaN nanowires on Si(111) *Appl. Phys. Lett.* **90** 2005–8

[20] Van Treeck D, Fernández-Garrido S and Geelhaar L 2020 Influence of the source arrangement on shell growth around GaN nanowires in molecular beam epitaxy *Phys. Rev. Mater.* **4** 1–14

[21] Vermeersch R, Jacopin G, Robin E, Pernot J, Gayral B and Daudin B 2023 Optical properties of Ga-doped AlN nanowires *Appl. Phys. Lett.* **122** 091106

[22] Pierret A, Bougerol C, Gayral B, Kociak M and Daudin B 2013 Probing alloy composition gradient and nanometer-scale carrier localization in single AlGaN nanowires by nanocathodoluminescence *Nanotechnology* **24**

[23] Jmerik V, Nechaev D, Orekhova K, Prasolov N, Kozlovsky V, Sviridov D, Zverev M, Gamov N, Grieger L, Wang Y, Wang T, Wang X and Ivanov S 2021 Monolayer-scale gan/aln multiple quantum wells for high power e-beam pumped uv-emitters in the 240–270 nm spectral range *Nanomaterials* **11**

[24] Gao N, Feng X, Lu S, Lin W, Zhuang Q, Chen H, Huang K, Li S and Kang J 2019 Integral Monolayer-Scale Featured Digital-Alloyed AlN/GaN Superlattices Using Hierarchical Growth Units *Cryst. Growth Des.* **19** 1720–7

[25] Nikishin S A, Holtz M and Temkin H 2005 Digital alloys of AlN/AlGaN for deep UV light emitting diodes *Japanese J. Appl. Physics, Part 1 Regul. Pap. Short Notes Rev. Pap.* **44** 7221–6

[26] MacMillan M F, Clemen L L, Devaty R P, Choyke W J, Asif Khan M, Kuznia J N and Krishnankutty S 1996 Cathodoluminescence of AlN-GaN short period superlattices *J. Appl. Phys.* **80** 2378–82

[27] Taniyasu Y and Kasu M 2011 Polarization property of deep-ultraviolet light emission from C-plane AlN/GaN short-period superlattices *Appl. Phys. Lett.* **99** 7–11

[28] Islam S M, Lee K, Verma J, Protasenko V, Rouvimov S, Bharadwaj S, Xing H and Jena D 2017 MBE-grown 232-270 nm deep-UV LEDs using monolayer thin binary GaN/AlN quantum heterostructures *Appl. Phys. Lett.* **110**

[29] Liu C, Ooi Y K, Islam S M, Verma J, Xing H, Jena D and Zhang J 2017 Physics and polarization characteristics of 298 nm AlN-delta-GaN quantum well ultraviolet light-emitting diodes *Appl. Phys. Lett.* **110**

[30] Liu C, Ooi Y K, Islam S M, Xing H G, Jena D and Zhang J 2018 234 nm and 246 nm

AlN-Delta-GaN quantum well deep ultraviolet light-emitting diodes *Appl. Phys. Lett.* **112** 1–5

[31] Kobayashi H, Ichikawa S, Funato M and Kawakami Y 2019 Self-Limiting Growth of Ultrathin GaN/AlN Quantum Wells for Highly Efficient Deep Ultraviolet Emitters *Adv. Opt. Mater.* **7** 1–7

[32] Koshelev O A, Nechaev D V., Brunkov P N, Orekhova K N, Troshkov S I, Ivanov S V. and Jmerik V N 2019 Suppression of Stark effect in ultra-thin stress-free GaN/AlN multiple quantum well structures grown by plasma-assisted molecular beam epitaxy *Journal of Physics: Conference Series* vol 1410

[33] Wang Y, Rong X, Ivanov S, Jmerik V, Chen Z, Wang H, Wang T, Wang P, Jin P, Chen Y, Kozlovsky V, Sviridov D, Zverev M, Zhdanova E, Gamov N, Studenov V, Miyake H, Li H, Guo S, Yang X, Xu F, Yu T, Qin Z, Ge W, Shen B and Wang X 2019 Deep Ultraviolet Light Source from Ultrathin GaN/AlN MQW Structures with Output Power Over 2 Watt *Adv. Opt. Mater.* **7**

[34] Aiello A, Wu Y, Pandey A, Wang P, Lee W, Bayerl D, Sanders N, Deng Z, Gim J, Sun K, Hovden R, Kioupakis E, Mi Z and Bhattacharya P 2019 Deep Ultraviolet Luminescence Due to Extreme Confinement in Monolayer GaN/Al(Ga)N Nanowire and Planar Heterostructures *Nano Lett.* **19** 7852–8

[35] Wu Y, Liu X, Wang P, Laleyan D A, Sun K, Sun Y, Ahn C, Kira M, Kioupakis E and Mi Z 2020 Monolayer GaN excitonic deep ultraviolet light emitting diodes *Appl. Phys. Lett.* **116**

[36] Kamiya K, Ebihara Y, Shiraishi K and Kasu M 2011 Structural design of AlN/GaN superlattices for deep-ultraviolet light-emitting diodes with high emission efficiency *Appl. Phys. Lett.* **99** 1–4

[37] Sun W, Tan C K and Tansu N 2017 AlN/GaN Digital Alloy for Mid- and Deep-Ultraviolet Optoelectronics *Sci. Rep.* **7** 1–8